Using electro-optic field mapping for design of dual-band circularly polarized active phased arrays

Conference Paper · April 2017

DOI: 10.1109/WAMICON.2017.8023961

Kazem Sabet
EMAG Technologies Inc.

K. Sarabandi
University of Michigan

Linda Katehi
University of California, Davis

USING ELECTRO-OPTIC FIELD MAPPING FOR DESIGN OF DUAL-BAND CIRCULARLY POLARIZED ACTIVE PHASED ARRAYS

Kazem Sabet, Richard Darragh, Ali Sabet
EMAG Technologies Inc.
Ann Arbor, MI 48108, USA

Kamal Sarabandi
The University of Michigan, Ann Arbor

Linda P.B. Katehi
The University of California, Davis

***Abstract*— Electro-optic (EO) probes provide an ultra-wideband, high-resolution, non-invasive technique for polarimetric near-field scanning of antennas and phased array systems. Unlike conventional near field scanning systems which typically involve metallic components, the small footprint all-dielectric EO probes can get extremely close to an RF device under test (DUT) without perturbing its fields. In this paper, we discuss and present measurement results for EO field mapping of a dual-band circularly polarized active phased array that operates at two different S and C bands: 2.1GHz and 4.8GHz. The array uses probe-fed, cross-shaped, patch antenna elements at the S-band and dual-slot-fed rectangular patch elements at the C-band. At each frequency band, the active phased array works both as transmitting and receiving antennas. The antenna elements have been configured as scalable array tiles that are arranged together to create larger apertures.**

Keywords—Phased Array; Field Measurement; Electro-Optic Probe; Radiation Pattern; Near-to-Far-Field Transformation

I. INTRODUCTION

The design of active electronically steered arrays (AESA) is a challenging, time-consuming and costly endeavor. The coupling effects among the radiating elements due to the propagation of substrate surface waves adversely affect the radiation pattern of the array and its scan characteristics. This problem is compounded for designing circularly polarized (CP) arrays when a good axial ratio performance is required over a wide angular field of view. The design process becomes much more sophisticated in the case of a dual-band circularly polarized active phased array. In the latter case, CP radiating elements at two different frequency bands occupy a shared aperture. As a result of this collocation, various types of coupling effects set into action not only among the radiating elements with the same resonant frequency, but also among adjacent elements resonating at different frequency bands. Current design processes that take into account various inter-element and intra-element coupling effects rely solely on computer simulations. In an anechoic chamber setting, it is possible to excite an individual radiating element and measure its active element pattern. However, such measurements do not shed light on the underlying coupling mechanisms. On the other hand, the conventional near-field scanning systems exhibit serious limitations for quantification of these coupling effects. This is mainly due to the invasive nature of their metallic probes, which act as receiving antennas and have to be placed far from the antenna under test (AUT) to avoid perturbing the latter's near fields [1]-[3].

A unique, versatile, near-field mapping technique has recently been introduced that circumvents most of the limitations mentioned earlier. This technique uses the linear Pockels effect in certain electro-optic crystals to modulate the polarization state of a propagating optical beam with the RF electric field penetrating and present inside the crystal [4]-[5]. What sets this system apart from conventional near-field scanning systems is the non-invasive nature of the all-dielectric optical probes, which are very small with a footprint of 1mm × 1mm and totally free of any metallic components. As a result, the probe can be placed very close to the surface of the AUT (less than 200μm away) and maps its near fields without perturbing them. In addition, due to the optical nature of these probes, ultra-wideband measurements are feasible.

In this paper, we present near-field and far-field measurement data for a dual-band circularly polarized active phased array that operates at two different S and C bands: 2.1GHz and 4.8GHz. The array uses probe-fed, cross-shaped, patch antenna elements at the S-band and dual-slot-fed rectangular patch elements at the C-band. It operates in half-duplex mode at both frequency bands. The designed and fabricated AESA features complete RF chains behind each individual radiating element including low-noise amplifiers, power amplifiers, T/R switches and digital phase shifters. The antenna elements have been configured as scalable array tiles that are patched together to create larger apertures. A satisfactory circular polarization performance have been demonstrated at both frequency bands. Both amplitude and phase of the field components are measured in each scan. From the scanned near field maps, the radiation pattern of the AUT is estimated using a near-to-far-field transformation [6]. The measurement results obtained using the electro-optic probes will be compared with full-wave simulation data as well as measured pattern data collected in an anechoic chamber.

II. THE ELECTRO-OPTIC FIELD PROBE

Imposing an external electric field on an electro-optic (EO) crystal induces a change in its refractive index, which then leads to a change in the polarization of an optical beam that passes through the EO crystal (linear birefringence) as shown in Figure 1. This in turn produces a measurable change in the optical intensity of the beam at a polarization analyzer [7]. The EO field probes are constructed from extremely small EO crystals

978-1-5090-4375-0/17/$31.00 ©2017 IEEE

mounted at the tip of an optical fiber. Figure 2 shows the photograph of a fiber-coupled EO field probe placed at a very low height above the surface of a dual-band AESA tile. The probe holder fixture is mounted on a computer-controlled XY translation stage that can scan the surface of the antenna tile.

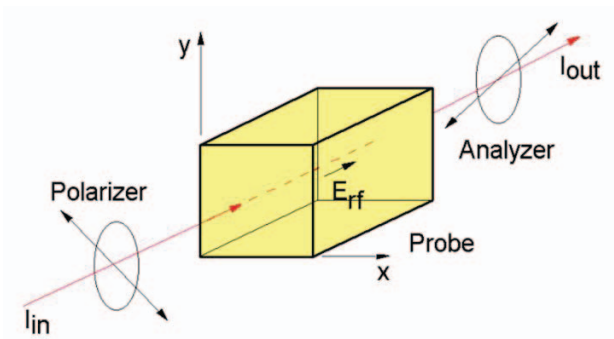

Figure 1: An optical beam propagating through an EO crystal and experiencing polarization change due to Pockels' effect.

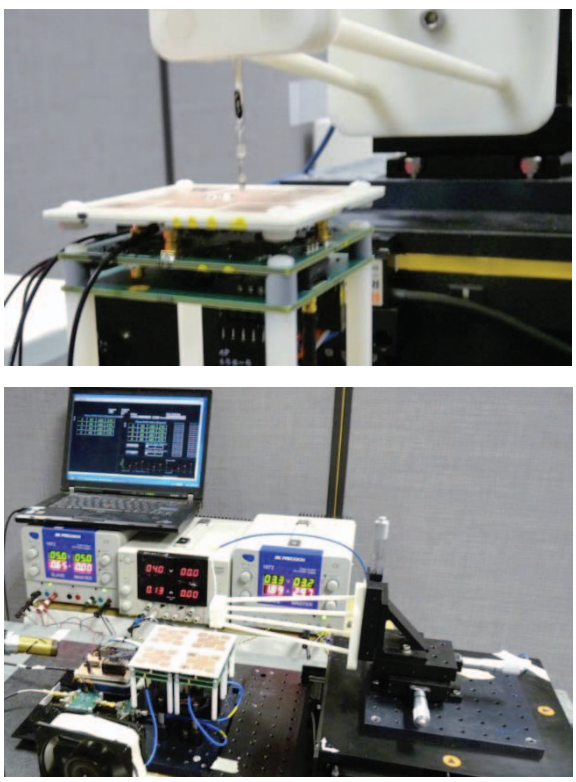

Figure 2: An EO probe mounted on an XY translation stage scanning the near fields of a dual-band AESA antenna.

The EO probe is connected via a polarization maintaining optical fiber to the optical mainframe of the NeoScan system [8], a turnkey electric field measurement system. This system can measure the amplitude and phase of the electric field simultaneously with a sub-millimeter resolution. The optically detected RF signal is down-converted to 100MHz and processed through a lock-in amplifier that is synchronized (phase-locked) with the signal generator or frequency synthesizer that feeds the AUT. The combination of the small probe size and non-metallic, all-dielectric parts leads to the ultimate RF non-invasiveness. Some of the key features of our field probe systems include:

- Broad measurement bandwidth (>20GHz) using the same optical probes
- High spatial resolution driven by the laser beam spot size (finer than 100 μm^2)
- Simultaneous amplitude and phase measurement
- Vectorial field measurement with very cross-polarization suppression better than 20dB

The EO field probes provide accurate multi-dimensional signal flow maps of RF, microwave and millimeter wave devices and circuits. Near-field maps of this kind can be very useful for investigation of inter-element coupling effects in antenna array structures, phase calibration of their aperture, or many other diagnostic applications. The near-field maps at slightly higher planes, where the device's evanescent, reactive fields decay sufficiently, can effectively be used to compute the far field radiation patterns of the AUT.

III. Dual-Band Circularly Polarized Active Phased Array For Nanosatellite Communications

A dual-band circularly polarized (CP) active phased array has been developed for nanosatellite communications. The AESA system operates as both transmitter and receiver at two different frequency bands: 2.1GHz (S-band) and 4.8GHz (C-band). The S-band CP radiating element consists of a probe-fed, cross-shaped patch with two orthogonal probe feed located close to the center of the cross. The C-band CP radiating element consists of a dual-slot-fed rectangular patch with two orthogonal edge slots located underneath the patch and excited by two microstrip lines, which are terminated in open quarter-wave stubs and are connected to the in-phase and quadrature ports of a hybrid branchline coupler. Each AESA tile contains one S-band cross patch and four satellite C-band rectangular patches with a total surface area of 65mm × 65mm.

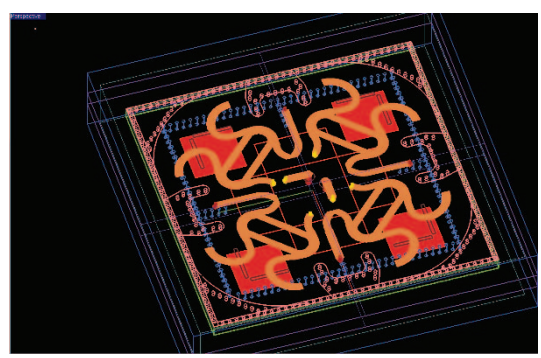

Figure 3: The unit cell of the dual-band circularly polarized AESA tile.

The tile consists of three vertically stacked printed circuit boards: the antenna board at the top, the C-band transceiver board sandwiched in the middle and the S-band transceiver board at the bottom. Miniature SMPM connectors are used to interconnect the boards. The entire design was developed using EM.Cube's FDTD Module [9]. Figure 3 shows the layout of the antenna board of the unit cell tile. Figures 4 and 5 show the

computed 3D radiation pattern of an aperture consisting of four AESA tiles at 2.1GHz and 4.8GHz, respectively. In the latter case, the beam of the C-band array has been steered at an elevation angle of 30° and an azimuth angle of 180°.

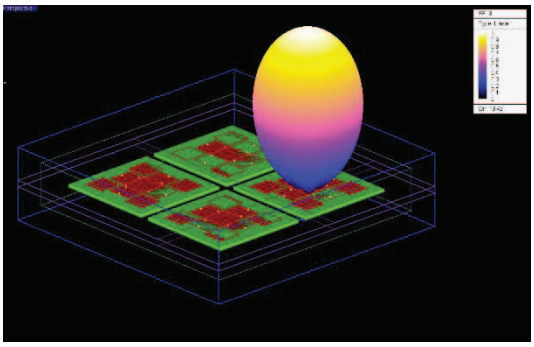

Figure 4: Computed 3D far field radiation pattern of the four-tile dual-band AESA array at 2.1GHz.

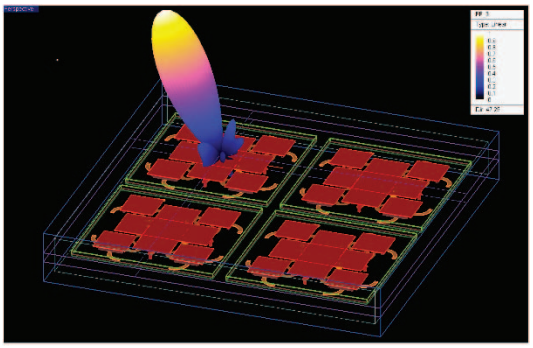

Figure 5: Computed 3D far field radiation pattern of the four-tile dual-band AESA array at 4.8GHz with scan angles θ = -30°, ϕ = 180°.

In each AESA tile, a 90° rotational phase progression is necessary among the four C-band patch elements to achieve circular polarization. The beam steering of the array is accomplished using a USB-controlled LabView interface that reads user supplied elevation and azimuth scan angles and translates them to 6-bit digital phase shift data. Each AESA tile integrates one S-band and four C-band 6-bit digital phase shifter devices within the two stacked transceiver boards. Using a network of T/R switches, the same phase shifters are shared by both transmit and receive chains in each transceiver board.

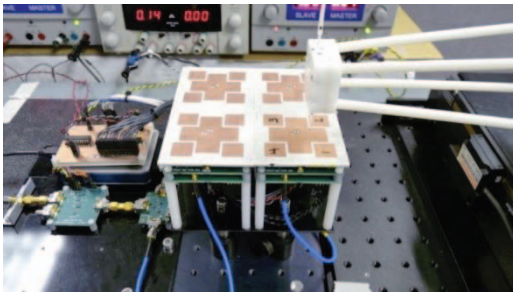

Figure 6: Computed 3D far field radiation pattern of the four-tile dual-band AESA array at 4.8GHz with scan angles θ = -30°, ϕ = 180°.

IV. Measurement Results

The dual-band circularly polarized (CP) AESA tile, whose design was described in the previous section, was fabricated and assembled. Four AESA tiles were next combined and arranged using a common carrier board to build a 2×2 S-band CP array and a 4×4 C-band CP array sharing a common aperture with a total surface area of 260mm × 260mm. Figure 6 shows the 4-tile assembly with the common carrier board and the USB controller device for changing the phase of the individual digital phase shifters.

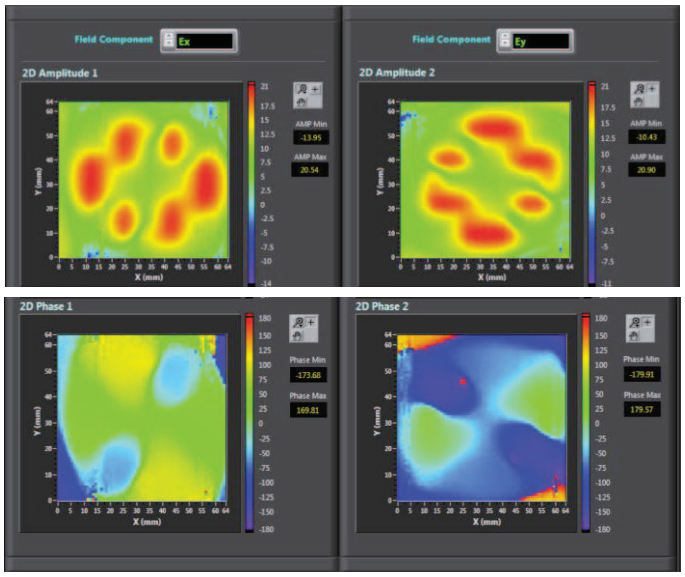

Figure 7: Measured electric field components above the surface of a single dual-band AESA tile at 2.1GHz. Top: Amplitude, Bottom: Phase. Left: Ex, Right: Ey.

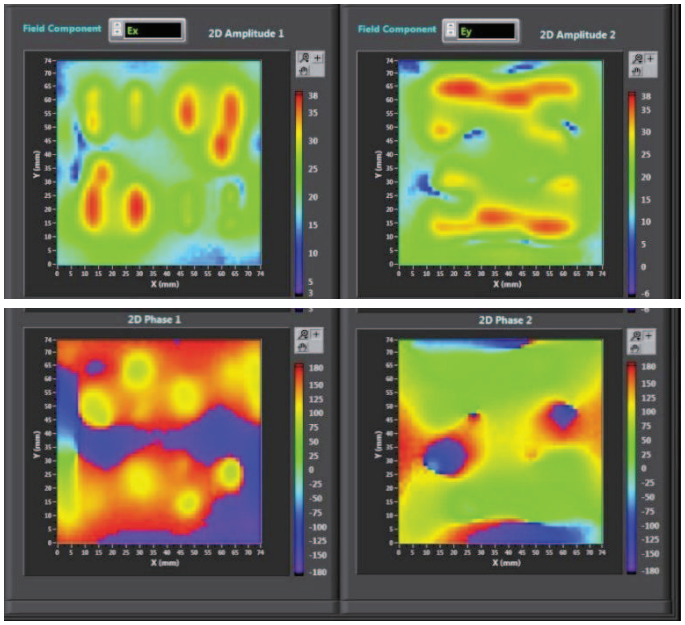

Figure 8: Measured electric field components above the surface of a single dual-band AESA tile at 4.8GHz. Top: Amplitude, Bottom: Phase. Left: Ex, Right: Ey.

First, the near-field maps of a single AESA tile were measured at a height of 2mm above the surface of the tile. Figure 7 shows the amplitude and phase maps of the tangential field components measured at 2.1GHz with the S-band cross patch excited. Figure 8 shows the amplitude and phase maps of the tangential field components measured at 4.8GHz with the four C-band patches excited and phase-shifted properly. Next, the amplitude and phase maps of the tangential field components above the surface of a 4-tile AESA assembly were measured at 4.8GHz with 16 C-band patches excited as shown in Figure 9.

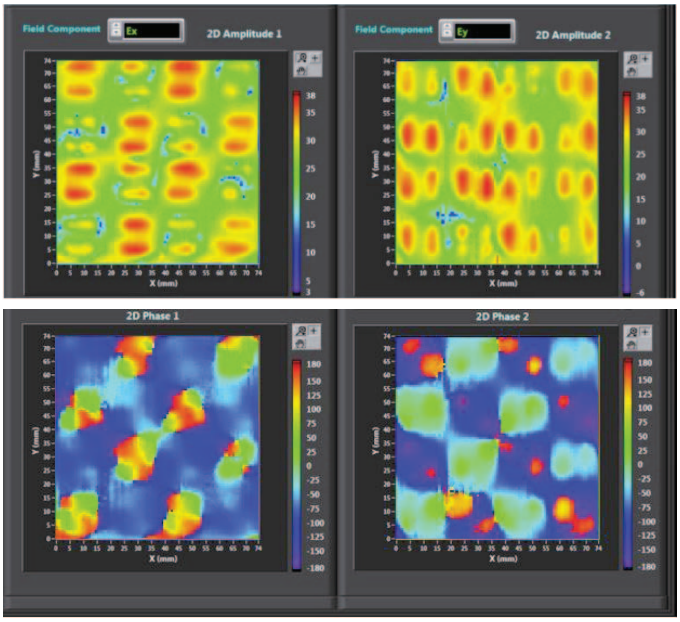

Figure 9: Measured electric field components above the surface of a four-tile dual-band AESA tile at 4.8GHz. Top: Amplitude, Bottom: Phase. Left: Ex, Right: Ey.

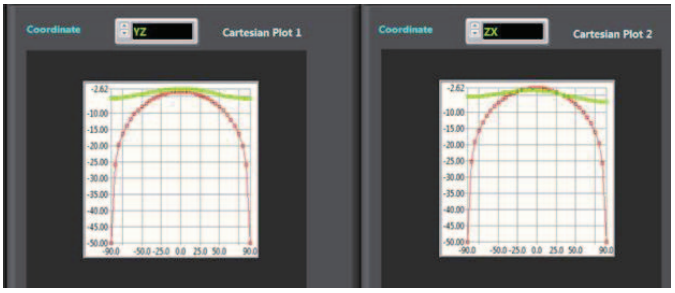

Figure 10: Measured principal-plane radiation patterns of a single dual-band AESA tile at 2.1GHz. Left: YZ plane, Right: ZX plane.

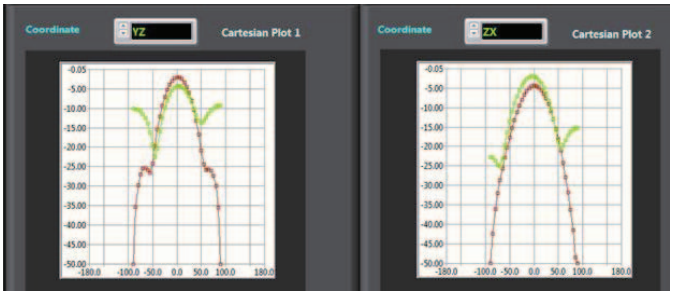

Figure 11: Measured principal-plane radiation patterns of a single dual-band AESA tile at 4.8GHz. Left: YZ plane, Right: ZX plane.

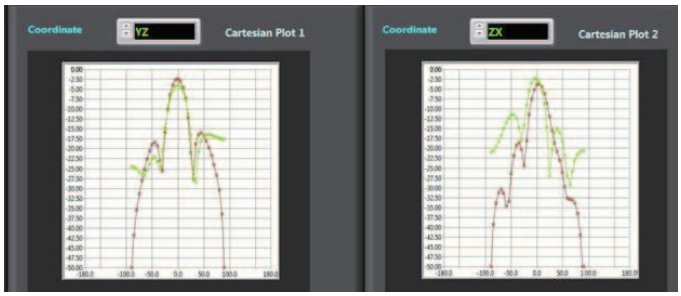

Figure 12: Measured principal-plane radiation patterns of a 4-tile dual-band AESA aperture at 4.8GHz. Left: YZ plane, Right: ZX plane.

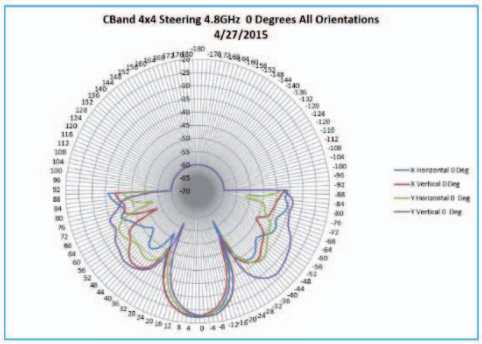

Figure 13: Measured principal-plane radiation patterns of the 4-tile dual-band AESA antenna at 4.8GHz in the anechoic chamber.

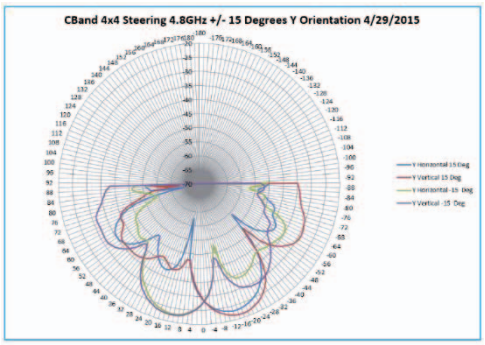

Figure 14: Measured principal-plane radiation patterns of the 4-tile dual-band AESA antenna at 4.8GHz with the array beam steered at an elevation scan angle of ±15°.

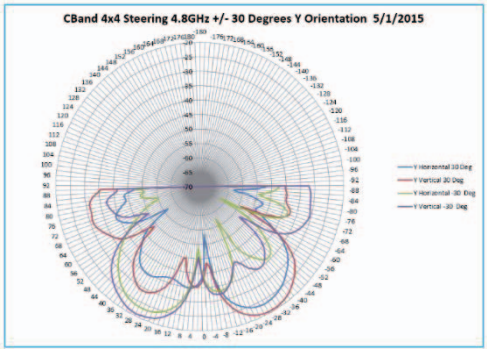

Figure 15: Measured principal-plane radiation patterns of the 4-tile dual-band AESA antenna at 4.8GHz with the array beam steered at an elevation scan angle of ±30°.

The NeoScan system uses the same near-to-far-field transformation that EM.Cube's FDTD Module utilizes for computation of the far field radiation patterns. The principal-plane radiation patterns of the single AESA tile were thus obtained at 2.1GHz and 4.8 GHz as shown in Figures 10 and 11, respectively. Good circular polarization is observed in both bands. Note that the C-band radiation patterns correspond to a 4-element planar array. Figure 12 shows the principal-plane radiation patterns of the assembly of four AESA tiles (as shown in Figure 6) measured at 4.8 GHz. A satisfactory circular polarization performance is again observed over a fairly large angular field of view.

The principal-plane radiation patterns of the dual-band CP AESA antenna were further measured at EMAG Technologies' in-house anechoic chamber for additional verification of the NeoScan system's results based on the near-field maps. Figures 13, 14, 15 and 16 show the principal-plane radiation patterns of the 4×4 C-band CP array measured at 4.8GHz in the chamber for different elevation scan angles of 0°, ±15° and ±30°, respectively. Note that positive and negative elevation scan angles in these figures denote those in the azimuth planes $\phi = 0°$ and $\phi = 180°$, respectively.

V. Conclusion

In this paper, we have used a wideband, non-invasive, electro-optic field probe to measure the near-field maps of a dual-band circularly polarized active phased array for nanosatellite communications. The near-field distribution profiles have been validated with FDTD simulation data. The far field radiation patterns of the AESA antenna were computed based on the near-field maps and were further verified using the measured radiation patterns of the same active array in an anechoic chamber. Additional measurement and simulation data will be presented at the conference.

References

[1] M. Hirose, S Kurokawa, and K. Komiyama, "Compact spherical near-field measurement system for UWB antennas," IEEE Intl. Symp. Antennas & Propagat. Digest, Washington DC, July 2005, pp. 692-695.

[2] A. Capozzoli, C. Curcio, G. D'Elia, and A. Liseno, "Phaseless antenna characterization by effective aperture field and data representations," IEEE Trans. On Antennas & Propagat., vol. AP-57, No. 1, January 2009, pp. 215-230.

[3] A. Capozzoli, C. Curcio, G. D'Elia, A. Liseno, P. Vinetti, M. Ameya, M. Hirose, S Kurokawa, and K. Komiyama, "Photonic pobes and advance (also phaseless) near-field far-field techniques," IEEE Antennas & Propagat. Mag., Vol. 52, No. 5, October 2010, pp. 232-241.

[4] K. Yang, G. David, J-G. Yook, I. Papapolymerou, L.P.B. Katehi, and J.F. Whitaker, "Electrooptic mapping and finite-element modeling of the near-field pattern of a microstrip patch antenna", IEEE Trans. on Microwave Theory & Tech., Vol. 48, No. 2, February 2000, pp. 288-294.

[5] K. Yang, t. Marshall, M. Forman, J. Hubert, L. Mirth, Z. Popovic, L.P.B. Katehi, and J.F. Whitaker, "Active-amplifier-array diagnostics using high-resolution electrooptic field mapping", IEEE Trans. on Microwave Theory & Tech., Vol. 49, No. 5, May 2001, pp. 849-857.

[6] C. A. Balanis, *Advanced Engineering Electromagnetics*, 2nd Ed., pp. 328-333, John Wiley & Sons, 2012.

[7] A. Yariv and P. Yeh, *Optical Waves in Crystals*, pp. 220-255, John Wiley & Sons, 1984.

[8] http://www.emagtech.com/wiki/index.php?title=NeoScan.

[9] http://www.emagtech.com/wiki/index.php?title=EM.Cube.